Photoinduced entanglement in a magnonic Floquet topological insulator

Satyaki Kar[1,*] and Banasri Basu[2,†]
[1]*Institute of Physics, Bhubaneswar - 751005, India*
[2]*Physics and Applied Mathematics Unit, Indian Statistical Institute, Kolkata - 700108, India*

(Received 10 July 2018; revised manuscript received 11 October 2018; published 13 December 2018)

When irradiated via high-frequency circularly polarized light, the stroboscopic dynamics in a Heisenberg spin system on a honeycomb lattice develops a next-nearest-neighbor (NNN) Dzyaloshinskii-Moriya (DM) type term, making it a magnonic Floquet topological insulator. We investigate the entanglement generation and its evolution on such systems, particularly an irradiated ferromagnetic XXZ spin-$\frac{1}{2}$ model in a honeycomb lattice as the system parameters are optically tuned. In the high-frequency limit, we compute the lowest quasienergy state entanglement in terms of the concurrence between nearest-neighbor (NN) and NNN pair of spins and witness the entanglement transitions occurring there. For the easy-axis scenario, the unirradiated system forms a product state but entanglement grows between the NNN spin pairs beyond some cutoff DM strength. Contrarily in the easy-planar case, NN and NNN spins remain already entangled in the unirradiated limit. It then goes through an entanglement transition which causes decrease (increase) of the NN (NNN) concurrences down to zero (up to some higher value) at some critical finite DM interaction strength. For a high frequency of irradiation and a suitably chosen anisotropy parameter, we can vary the field strength to witness sudden death and revival of entanglement in the Floquet system. Both exact diagonalization and modified Lanczos techniques are used to obtain the results up to 24 site lattice. We also calculate the thermal entanglement and obtain estimates for the threshold temperatures below which nonzero concurrence can be expected in the system.

DOI: 10.1103/PhysRevB.98.245119

I. INTRODUCTION

Recently, there is an upsurge of interest in realizing and utilizing quantum information aspects of various quantum many-body systems (QMBS). Built at the interface of quantum information science, condensed matter theory, statistical physics, and quantum field theory, the study of many-body entangled states rapidly has become a very active topic of research. In this respect, quantum entanglement plays a crucial role in the highly efficient quantum computation and quantum information processing [1,2]. With the rapid development of the experimental process on quantum control, there is a rapidly growing interest in entanglement generation. Thus, the quantification of entanglement has found a key place in quantum information process applications.

On the other hand, recent study of Dirac and topological magnons in solid-state magnetic systems [3–7] is expected to open a challenging avenue towards magnon spintronics and magnon thermal devices. Since the magnons are charge-neutral quasiparticles, it is believed that the magnon quantum computing will offer a favorable pathway for eliminating the difficulties posed by charged electrons [8,9] and, as such, the magnonic devices would be more efficient in quantum memory and information storage [10–13].

In this context, our focus is to study the entanglement in a magnonic system that is irradiated via a strong periodic circularly polarized light. There are many measures of entanglement, such as entanglement entropy, entanglement of formation, purity or negativity capturing the quantum correlation within an interacting system by different means. Von Neumann entropy gives a standard measure for entanglement of pure states. But, for a generic mixed state, an entanglement entropy can give nonzero values for each of the subsystems even if there is no entanglement. So, in those cases it is the entanglement of formation that gives a true measure of entanglement [14]. For a given purity or mixedness, with different possible combination of pure states that the state can collapse into, it is the entanglement of formation that gives the minimum number of singlets required to create the mixed density of states. This is a monotonically increasing function of an argument called concurrence C, with $0 \leqslant C \leqslant 1$, which by itself can also be regarded as a measure for entanglement in a mixed state, for example, between a pair of qubits within a multiqubit large system [14]. In fact, this is an entanglement monotone which is zero for separable states and unity for Bell states (four maximally entangled two-qubit states). For a pair of qubits, concurrences are well defined as will be described later. Our analysis shows their tunability in terms of the frequency of irradiation and provides significant control over the quantum information processing.

At the very outset, let us reiterate here that recent trends show plenty of work on optical lattices involving Dirac plasmons [15], Dirac magnons [7], or photonic topological insulators [16] that have Dirac-type bosonic spectrum. When dynamics is studied in such systems in presence of time-varying fields, a plethora of exotic phenomena such as defect productions, dynamical freezing, dynamical phase transition,

*satyaki.phys@gmail.com
†sribbasu@gmail.com

or entanglement generation [17–20] can be expected. Particularly for a periodic quench, one can use the Floquet theory [21] for stroboscopic evolution [22] of the system, which results in an effective static Hamiltonian out of the originally dynamical system.

A Dirac system shows interesting dynamical features upon light irradiation [23–34]. An irradiated field can lead to nontrivial Floquet systems like Floquet topological insulators (FTI) [23], as can be seen, for example, in an irradiated semiconductor quantum well [24] or a three-dimensional (3D) topological insulator [25]. We know that a ferromagnetic Heisenberg spin-$\frac{1}{2}$ (FMHS) model with next-nearest-neighbor (NNN) Dzyaloshinskii-Moriya interaction (DMI) in a honeycomb lattice, under a linear spin-wave approximation (LSWA), turns out to be a magnonic equivalent of the Haldane model, the famous primitive toy model to show topological transitions [35]. Interestingly, this can also be achieved via irradiation with high-frequency circularly polarized light [36]. The resulting Floquet Hamiltonian develops easily tunable synthetic laser-induced NNN DMI in addition to a FMHS with modified anisotropy. Within LSWA, the model behaves like a bosonic Haldane model enabling the system to emerge as topologically nontrivial at intermediate frequencies of the irradiation.

In this paper, we probe the entanglement characteristics of such Floquet model, born out of irradiating the spin system, both in their topologically trivial and nontrivial limits. In the infinite-frequency limit (which is equivalent to zero DMI), the resulting lowest quasienergy state is a ferromagnetic product state and hence unentangled, unless the anisotropy is of easy-planar type. But, with moderately high frequencies (but not small ones, as discussed in Appendix A for which other higher-order terms from the high-frequency expansion of the Floquet Hamiltonian also become relevant), the system can become entangled due to generation of the DMI term, as an antisymmetric DM exchange interaction can excite entanglement and teleportation fidelity [37] in the system. This is a short-range interacting system and thus the entanglement transitions do not coincide with the topological transition that occurs as soon as DMI term is brought in. However, deep within the topological phase, the system shows finite entanglement, irrespective of the value of anisotropy.

While dealing with low-temperature entanglement of these systems, we not only need information of the lowest-energy state, but that of low-energy excitations as well. Following that, a measurement on thermal entanglement is very effective in this context. We compute thermal concurrences in our Floquet model and notify its behavior at the various low temperatures.

For numerical computation, we use diagonalization methods like exact diagonalization (for small lattices with $L = 6$ and 12) and a modified Lanczos technique [38] (for $L = 18$ and 24) and obtain the concurrences there from.

The paper is organized as follows. In Sec. II, we start with the Hamiltonian formulation of the problem. In Sec. III, we introduce concurrences in the Floquet model and discuss briefly how to compute that. Section IV details our results and the corresponding discussion, and finally in Sec. V, we conclude our work.

II. HAMILTONIAN FORMULATION

A ferromagnetic spin-$\frac{1}{2}$ XXZ model is given as

$$H_J = -J \sum_{\langle i,j \rangle} \left[S_i^z S_j^z + \frac{\Delta_0}{2} (S_i^+ S_j^- + \text{H.c.}) \right]. \tag{1}$$

When such system is irradiated with light, the electric field ($\mathbf{E}$) of the light interacts with the spin moments (μ) yielding time-periodic Aharonov-Casher phases [39] $\phi_{ij} = \frac{1}{\hbar c^2} \int \mathbf{E} \times \mu \cdot dx_{ij}$ between sites i and j in the lattice. This paves the way for a Floquet analysis resulting in an effective static Hamiltonian for the dynamic system. Particularly for high-frequency circularly polarized irradiation with $E = E_0(\cos \omega t, \sin \omega t)$, a high-frequency expansion can lead us to a Floquet Hamiltonian given as

$$\begin{aligned} H_F &= -J \sum_{\langle i,j \rangle} \left[S_i^z S_j^z + \frac{\Delta_\alpha}{2} (S_i^+ S_j^- + \text{H.c.}) \right] \\ &\quad + D_\alpha(\omega) \sum_{\langle\langle i,k \rangle\rangle} \nu_{ik} \left(S_i^x S_k^y - S_k^x S_i^y \right) \\ &= -J \sum_{\langle i,j \rangle} \left[S_i^z S_j^z + \frac{\Delta_\alpha}{2} (S_i^+ S_j^- + \text{H.c.}) \right] \\ &\quad + \frac{D_\alpha(\omega)}{2} \sum_{\langle\langle i,k \rangle\rangle} \nu_{ik} (i S_i^+ S_k^- + \text{H.c.}). \end{aligned} \tag{2}$$

The details of the calculation can be found in Appendix A. Notice that the spin anisotropy gets altered from Δ_0 to $\Delta_\alpha = J_0(\alpha)\Delta_0$ thereby changing the spin anisotropy parameter in the Floquet model. Here, $J_n(\alpha)$ is the nth-order Bessel's function of first kind with $\alpha = \frac{g \mu_B a E_0}{\hbar c^2}$ (see Appendix A for definition of the parameters). Furthermore, an additional NNN DMI term sets in having amplitude $D_\alpha(\omega) = K(\alpha)/\omega$ where $K(\alpha) = \sqrt{3}\Delta_0^2 J^2 J_1(\alpha)^2$. So, for very large ω, this is essentially zero and can only become significant otherwise. This DMI term acts as a complex NNN hopping term, like in a spinless Haldane model, and is the reason behind its topological nontriviality. Here, ν_{ik} is a prefactor for hopping between sites i and k and $\nu_{ik} = +1\ (-1)$ for $i, k \in A\ (B)$ sublattice of the system.

III. CONCURRENCE IN FLOQUET MODEL

In order to compute the concurrence of the ground state as well as low-energy excitations of a system, we need the full energy spectrum of the problem and we use numerical diagonalization of the Hamiltonian matrix to serve that purpose. As we deal with a Floquet model here, we look out for the Floquet quasienergy spectrum and, particularly, the lowest quasienergy state and concurrences therein.

We first briefly describe the lattice, its site numbering and its bond connections, that are necessary to identify different interaction pairs. A honeycomb lattice [see Fig. 1(a)] can more conveniently be described using a brick-wall lattice. First, we use periodic boundary condition (PBC) and the site numbering is given accordingly. The example for $L = 18$ site lattice can be seen in Fig. 1(b). For computing concurrence between NN and NNN pairs, we considered the numbered pairs (3,4) and (3,11), respectively. Please note here that this numbering

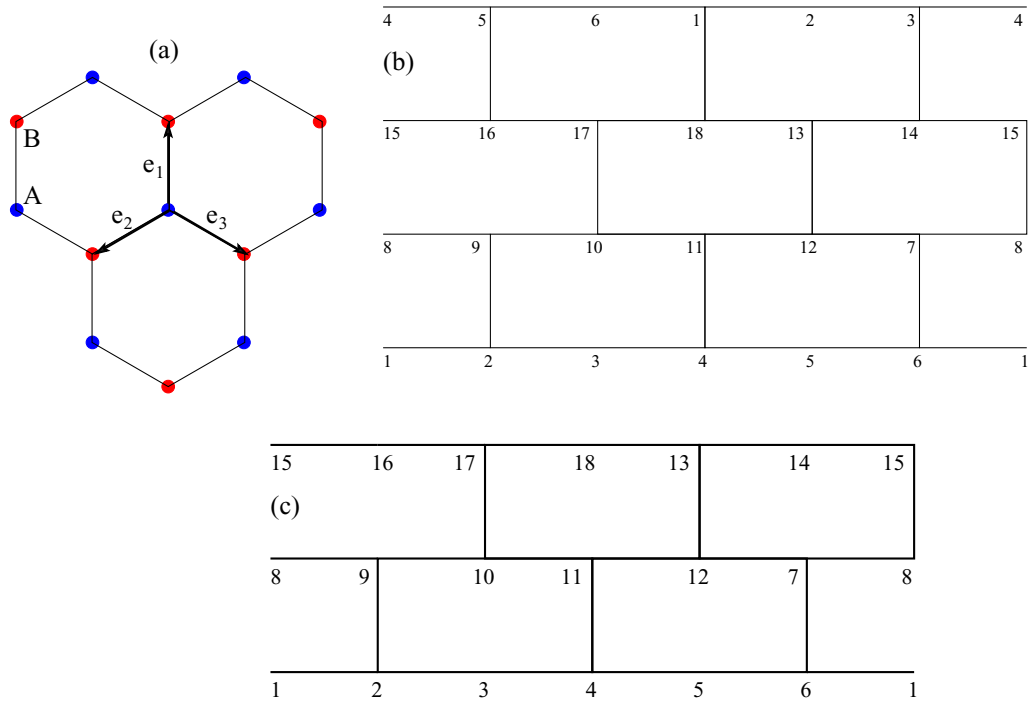

FIG. 1. (a) Honeycomb lattice containing sublattices A and B. Unit vectors $\mathbf{e_1}$, $\mathbf{e_2}$, and $\mathbf{e_3}$ (see Appendix A) are shown as well. Site numbering, implementing (b) PBC and (c) OBC, in a brick-wall lattice (which is topologically equivalent to a honeycomb lattice) of size $L = 18$. The odd (even) numbered sites fall within the sublattice A (B).

is not unique and we only need to ensure that the numbering and boundary conditions do not break the symmetry of the lattice and treat each of the hexagonal plaquettes equally. In order to see the effect on entanglement at the edges, later we also consider finite systems using open boundary conditions (OBC) along y directions. As can be seen from Fig. 1(c), this amounts to a pair of (zigzag) edges parallel to the x direction while the system effectively extends to infinity along x following the usual PBC (like in a nanoribbon).

Our paper deals with systems of lattice size $L = 6,\ 12,\ 18$, and 24, respectively. Due to numerical constraints, we use exact diagonalization only for smaller 6 and 12 site lattices while for $L = 18$ and 24, we use a modified Lanczos technique [38]. This latter method search for the ground state (a lowest quasienergy state, in this case) starts from a random state ψ_0, with nonzero overlap with the ground state. This is then acted upon by the Floquet Hamiltonian H_F to obtain the state $\psi_0' = \frac{H_F\psi_0 - \langle H_F\rangle\psi_0}{\sqrt{\langle H_F^2\rangle - \langle H_F\rangle^2}}$, which is orthogonal to ψ_0. The Hamiltonian, in its 2×2 representation spanned by the basis states ψ_0 and ψ_0', is then diagonalized. The lowest eigenstate is renamed as ψ_0 and iterations are continued until the true minimum energy state is obtained. See Ref. [38] for details.

Given the state, we can now compute the concurrence between NN or NNN spins. Let us call the spin-z basis vectors as $|\phi_j\rangle$'s, in terms of which we can write the eigenstates of our Hamiltonian as $|\psi_i\rangle = c_{ij}|\phi_j\rangle$ and let E_i denote the ith eigenvalue. The ground-state density matrix will then be given by $\rho_G = |\psi_0\rangle\langle\psi_0|$. We can also compute the thermal density matrix which, in the canonical ensemble, is given by $\rho_T = \frac{1}{Z}\sum_i e^{-\beta E_i}|\psi_i\rangle\langle\psi_i|$, with $Z = \sum_i e^{-\beta E_i}$.

As the system is bipartitioned into subsystems a and b, we can write $|\phi_i\rangle = |\phi_i^a\rangle \otimes |\phi_i^b\rangle$ and the reduced density matrix in the subsystem a will be given as

$$\rho^R_{i_a j_a} = \frac{1}{Z}\sum_{k,i_b,j_b} c^\star_{ki} c_{kj} e^{-\beta E_k}\delta_{\phi_i^b,\phi_j^b}. \tag{3}$$

Our subsystem a consists of a pair of spins, especially NN or NNN pairs, that we consider here. We should mention here that our work involves bipartite entanglement alone and does not deal with entangled states (like a GHZ state or a W state) corresponding to further partitioning of systems.

Now, let us look at the definition of quantum concurrence. For a two-qubit system, the pure state $|\psi\rangle$ contains a measure of concurrence $C(|\psi\rangle) = |\langle\psi|\tilde{\psi}\rangle|$, where $|\tilde{\psi}\rangle$ is the time-reversed state of $|\psi\rangle$. For a spin system, a time-reversed state is the spin-flipped state and for a spin-$\frac{1}{2}$ (two-qubit) system it is given by $|\tilde{\psi}\rangle = (\sigma_1^y \otimes \sigma_2^y)|\psi^\star\rangle$. When we have a general mixed state, full information of the wave function is not available and the time-reversed density matrix is obtained instead, as $\tilde{\rho}^R_{12} = (\sigma_1^y \otimes \sigma_2^y)\rho^{R^\star}_{12}(\sigma_1^y \otimes \sigma_2^y)$, to compute the concurrence. Here, ρ^R_{12} denotes the reduced density matrix at the reduced two-qubit level. Concurrence becomes a function of ρ^R_{12} and can be shown [14] to be given by

$$C(\rho) = \max\{0, \lambda_1 - \lambda_2 - \lambda_3 - \lambda_4\}, \tag{4}$$

where λ_i's denote the square root of eigenvalues of $R_{12} = \rho^R_{12}\tilde{\rho}^R_{12}$ in descending order.

IV. RESULTS AND DISCUSSION

First, we study the effect of anisotropy or Δ_α at $\omega \to \infty$ limit, i.e., the anisotropic Heisenberg ferromagnetic spin system alone. Within the lowest quasienergy state, we

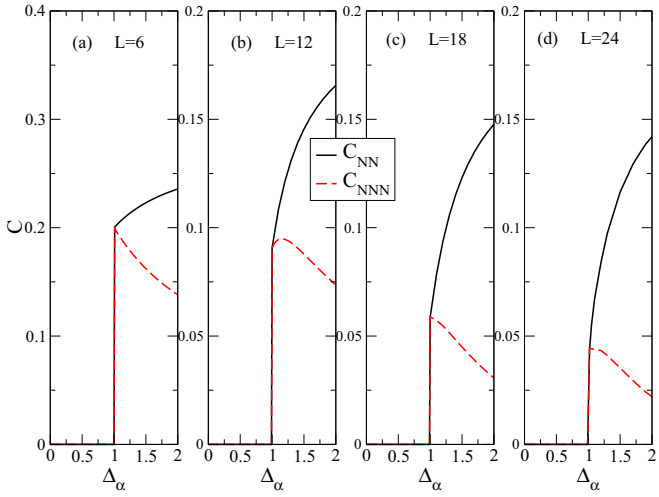

FIG. 2. C_{NN} and C_{NNN} versus Δ_α at $\omega \to \infty$ limit for $L = 6,\ 12,\ 18$, and 24, respectively.

probe the concurrence between nearest-neighbor sites (C_{NN}) and that between next-nearest-neighbor sites (C_{NNN}) of the Floquet model. See Fig. 2 for results of C vs Δ_α for lattices with $L = 6,\ 12,\ 18$, and 24. Physically, variation of Δ_α can be achieved by varying Δ_0, keeping α fixed. We see that concurrence becomes nonzero abruptly at $\Delta_\alpha = 1$, signaling an entanglement transition. This feature remains intact in the thermodynamic limit as well, as shown via finite-size scaling in Appendix B. However, the jump/discontinuity reduces as lattice size is increased.

Next, we consider the situation as the DMI is turned on, with decrease of ω to finite large values. We see the concurrence C_{NNN} to appear and then increase gradually beyond some cutoff $D_\alpha(\omega)$ values for $\Delta_\alpha < 1$ whereas C_{NN} always remains zero. That cutoff remains the same as long as the Ising anisotropy remains. For $\Delta_\alpha \geqslant 1$, the system is already entangled at $D_\alpha(\omega) = 0$. There is also a cutoff $D_\alpha(\omega)$ strength in this case, beyond which C_{NN} perishes and C_{NNN} shoots up and keep on increasing to reach a plateau finally. We should mention here that for a fixed α, $D_\alpha(\omega)$ is inversely proportional to ω and as such $D_\alpha(\omega)$ can be replaced with ω^{-1} to visualize the frequency dependence of the concurrences more clearly. Accordingly, Fig. 3 shows variation of concurrences in terms of ω^{-1} in units of the prefactor $K(\alpha)$.

Now, let us explain the results of concurrence that we get. At very large frequency, the DMI term becomes negligible and the XXZ model of the Floquet Hamiltonian shows finite entanglement as soon as the anisotropy becomes easy planar. The product state of the easy-axis ferromagnet (FM) turns into a entangled state with moments oriented in the spin-xy plane [40]. Finally, for $\Delta_\alpha \to \infty$, the ground state still has no product state form as no direction in the xy plane is preferred for the spin moments. As a result, the entanglement, emerging from $\Delta_\alpha \to 1+$, gradually saturates to a finite value for large Δ. With $\omega \to \infty$ [or, $D_\alpha(\omega) = 0$], there is no direct interaction between NNN spins. The Heisenberg point being the critical point, spin correlation is at its peak for closest spins, which then decays as the distance between the spins is increased. Hence, both NN and NNN spins are very much correlated as well as entangled at $\Delta_\alpha = 1$. Moreover, as the

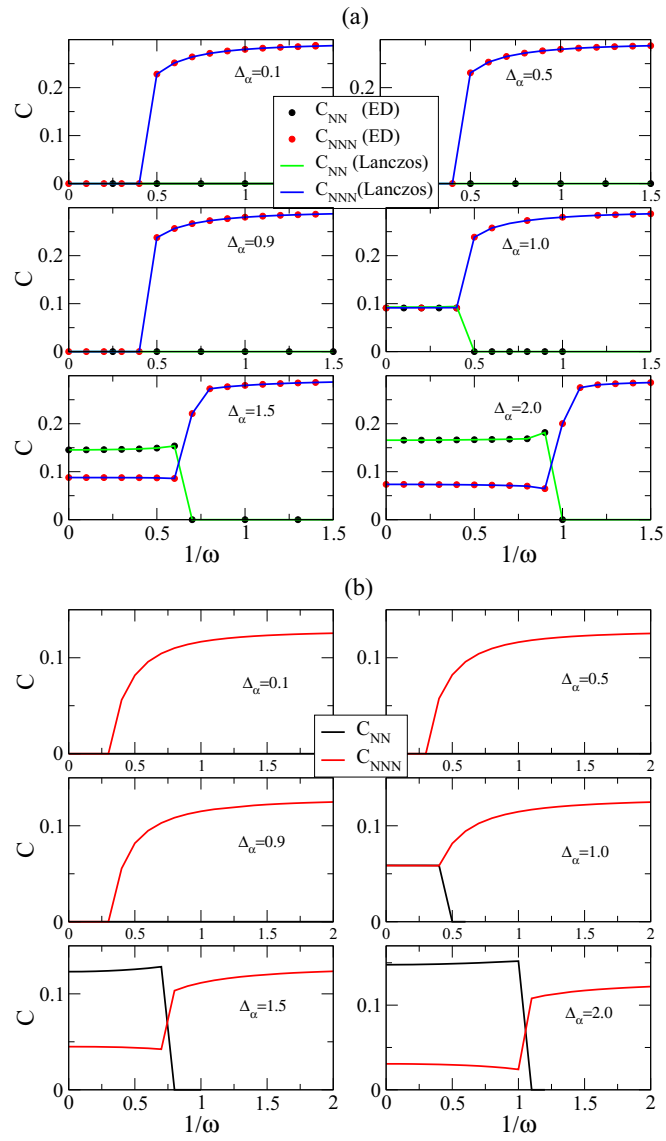

FIG. 3. Concurrence versus $1/\omega$ [in units of $K(\alpha)$] for (a) $L = 12$ and (b) $L = 18$. In (b), results are obtained using modified Lanczos technique whereas in (a) both exact diagonalization (circles) and Lanczos (lines) results are shown.

entanglement producing spin-fluctuation terms appears only between NN spins, we find $C_{NN} > C_{NNN}$ whenever they are nonzero. We should emphasize here that as spin exchange between NN pairs entangles them more, we see C_{NN} to increase steadily with Δ_α beyond the Heisenberg point. This pushes C_{NNN} for steady decrease possibly due to spin conservation or the monogamy of entanglement [41]. Let us add here that the bump in C_{NNN} observed for $\Delta_\alpha \to 1+$ at $L = 12$ is a finite-size effect which gets wiped off significantly in the plot corresponding to $L = 18$ and 24. Notice that it does not appear for $L = 6$ as PBC makes this a special case where the NN and third-NN sites often become identical.

Now, as the DMI term is turned on, due to decrease of the frequency of irradiation from very large values, the system becomes topological. However, it takes some finite $D_\alpha(\omega)$ values to get the Floquet system with easy-axis anisotropy to become entangled for NNN spin pairs. This is because

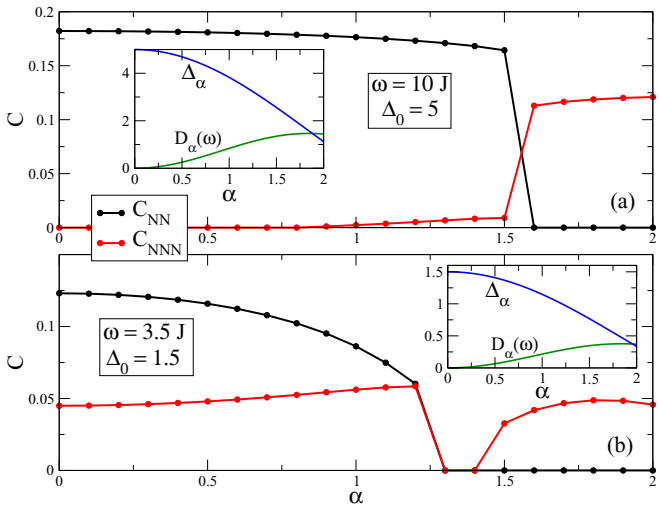

FIG. 4. Variation of C_{NN} (black) and C_{NNN} (red/gray) as a function of α on a $L = 18$ size lattice for (a) $\omega = 10J$ and $\Delta_0 = 5$ and (b) $\omega = 3.5J$ and $\Delta_0 = 1.5$. The inset shows the variation of Δ_α and $D_\alpha(\omega)$ with α.

the NNN spin-fluctuation terms oppose the FM ordering and it takes a finite threshold to disrupt that ordering and set in entanglement. On the other hand, the NN pairs never get entangled by introduction of this complex NNN hopping term. The easy-plane ferromagnet, which had finite C_{NN} and C_{NNN}, shows decrease and increase in entanglement with $D_\alpha(\omega)$ for NN and NNN pairs, respectively. The DMI term is a precursor of the spin-orbit coupling in the system and it favors spin canting. As this term acts between NNN pairs, a strong $D_\alpha(\omega)$ indicates a larger correlation among the NNN pairs. But, it also competes with NN spin exchange term and lets the correlation between the NN pairs perish gradually. Figure 3(a) shows the concurrence results for $L = 12$ where both exact diagonalization and Lanczos results are shown, which fairly match for the values of anisotropies considered. For larger $L = 18$ site lattice, we use the Lanczos method and obtain the same qualitative results as shown in Fig. 3(b). Notice that for the easy-planar case, C_{NNN} shows two smooth branches connected by a jump/discontinuity in the middle [however, such high-frequency branch vanishes for very large Δ_α, as also can be seen in Fig. 4(a) which shows $C_{\mathrm{NNN}} = 0$ for small α's]. Using finite-size scaling analysis, we have seen this to exist even in the thermodynamic limit (see Appendix B). This is a phase transition in which a redressing of the spins develops within the spin-xy plane. An easy-planar ferromagnet already has entangled NN and NNN spin pairs even without any DMI term. With finite ω, DMI is brought in which opposes the existing NNN spin ordering (and that enhances C_{NN} accordingly due to monogamy of entanglement) resulting in slight reductions in C_{NNN} with ω. On the other hand, the low-ω or large-$D_\alpha(\omega)$ branch of the plot appear beyond the cutoff $D_\alpha(\omega)$ strength, like in the easy-axis case, and characterizes the increase in NNN spin correlation (in its DMI induced new spin ordering) with $D_\alpha(\omega)$ or ω^{-1}. Our results on C-vs-$1/\omega$ plots describe variation of concurrences as the $D_\alpha(\omega)$ is varied, keeping α fixed. But, it is also useful to look at the variation of concurrences with α (see that α is proportional to the electric field amplitude E_0) for fixed large ω values. In Fig. 4 we can see such variations for two different sets of (ω, Δ_0). In Fig. 4(a) and within the range of α shown, easy-planar anisotropy is experienced by the Floquet system. It shows that a large anisotropy Δ_α can push C_{NNN} to zero even at the unirradiated limit $\alpha = 0$. In Fig. 4(b), we consider a comparatively small ω, yet being large compared to J and $\Delta_0 J$. It shows transition from easy-planar to easy-axis anisotropy (see the inset). With increase of α, the anisotropy Δ_α changes from easy-planar to easy-axis type (beyond $\alpha = 1.2$) and that makes C_{NN} to go to zero for all larger α values, whereas the behavior of C_{NNN} demonstrates aptly the sudden death and revival of entanglement [42] as it remains zero only if the $D_\alpha(\omega)$ is less than the cutoff value as mentioned in the discussion pertaining to Fig. 3.

A. Thermal entanglement

We know that the ground state is realized at zero temperature and, in practice, low-energy excitations also need to be taken into account to understand the low-temperature phenomena in a system. Thus, in our case, it is wise to take a look at the thermal entanglement that corresponds to entanglement properties at a finite temperature. Figure 5 shows the results of thermal concurrences C_{NN} and C_{NNN} in a $L = 12$ size system

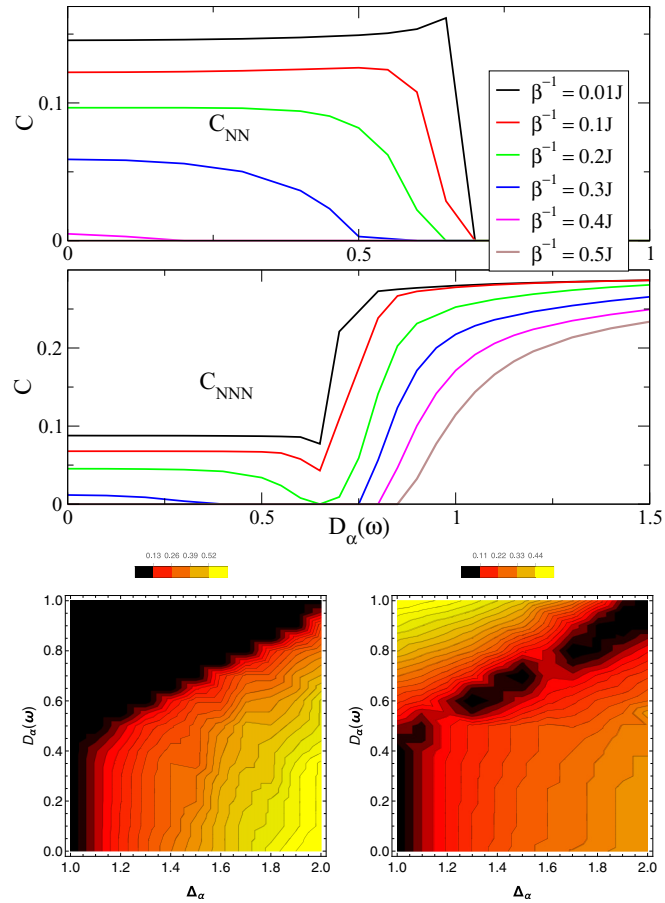

FIG. 5. (Top) Thermal concurrence for $L = 12$ at $\Delta_\alpha = 1.5$. Threshold temperature T_{th} for C_{NN} (bottom left) and C_{NNN} (bottom right) in the $D_\alpha(\omega) - \Delta_\alpha$ plane.

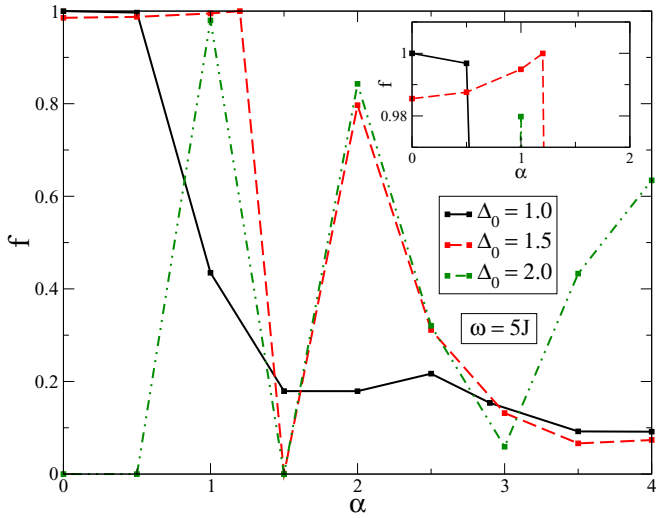

FIG. 6. Variation of fidelity of the lowest quasienergy state between the edgeless and edged configurations corresponding to $\Delta_0 = 1.0,\ 1.5$, and 2.0 and $\omega = 5J$ at $L = 18$. The inset shows the same plot zoomed in around $f = 1$.

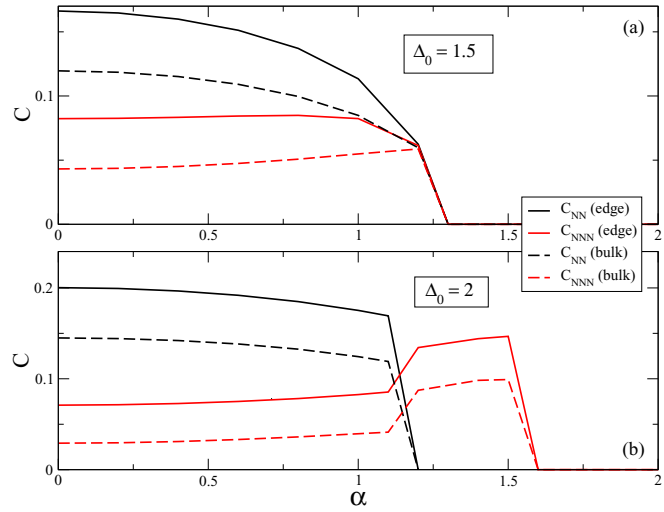

FIG. 7. $C_{\rm NN}$ (black) and $C_{\rm NNN}$ (red/gray) versus α at the edges (solid lines) and within the bulk (dashed lines) of a $L = 18$ size lattice with PBC along x and OBC along y for $\omega = 5J$ and for (a) $\Delta_0 = 1.5$ and (b) $\Delta_0 = 2.0$, respectively.

obtained for various β $(= \frac{1}{k_B T})$ values, and for $\Delta_\alpha = 1.5$. Our thermal entanglement results show that temperature causes the entanglement measure in the system to wear off and, with high temperature, the thermal fluctuation leads the system towards complete unentanglement. As further quantification, we compute the threshold temperature $T_{\rm th}$ above which there is no concurrence possible in the Floquet states. In bottom panel of Fig. 5, we show the variation of $T_{\rm th}$ for $C_{\rm NN}$ and $C_{\rm NNN}$ in a $D_\alpha(\omega) - \Delta_\alpha$ plane. It shows that a large Δ_α (i.e., much larger than unity) keeps the NN spins entangled up to some appreciably large-$T_{\rm th}$ values, if the irradiation born $D_\alpha(\omega)$ term is not very strong. On the other hand, a large $D_\alpha(\omega)$ makes the NNN spins entangled with appreciably large-$T_{\rm th}$ values when easy planar Δ_α is not very large.

B. Results for finite geometries with edges

As the presence of the DMI term brings in topological nontriviality to the Floquet problem, we need to pay special attention to the edges. Hence, we consider finite-size clusters with PBC along x and OBC along y so as to produce nanoribbon geometries with zigzag edges at the top and bottom along the x direction and try to quantify the edge correlations in the system. First, we calculate the fidelity f (i.e., wave-function overlap) between the lowest quasienergy states of an edgeless (with PBC along x and y) and edged (with PBC along x, OBC along y) system (for $L = 18$) as H_F is optically tuned keeping ω fixed. A few results are shown in Fig. 6 for isotropic as well as easy-planar configurations. The oscillating behavior appears due to the presence of Bessel's functions within the Hamiltonian parameters. At Heisenberg point, we witness $f = 1$ in the unirradiated limit, implying identical states for the edged and edgeless configurations. Hence, like any property, entanglement measures also do not change by merely bringing in such edges. But, larger anisotropies (like $\Delta_0 = 1.5,\ 2.0$, as shown in Fig. 6) causes states to differ even in the unirradiated limit and we get different measures for concurrences for edge spin pairs and bulk spin pairs (see Fig. 7). Particularly, if we look at the variation of $C_{\rm NN}$ and $C_{\rm NNN}$ with DMI strength $D_\alpha(\omega)$ for fixed Δ_α values (see Fig. 8), we find larger estimates for concurrences for edge spin pairs as compared to that for a bulk pair, even though the qualitative features of the two cases do not show any discernible difference. We identify this as an edge effect and suspect that the reduction of coordination numbers for the spins at edges can amount to further entangling of the edge pairs as a result of monogamy of entanglement [41]. We reiterate here that our fidelity calculation can only indicate identical or nonidentical lowest quasienergy state entanglement behaviors depending on whether $f = 1$ or $f \neq 1$. For $\alpha \neq 0$, we obtain $f \neq 1$ in general and different entanglement measures can be expected for the edged configuration. As long as $\Delta_\alpha = 1$, our results show full fidelity (see Fig. 6 and the corresponding entanglement match in Fig. 7). We can say that for those cases, edge states are not present in the lowest quasienergy states of the FTI. Other than those points, we witness both $C_{\rm NN}$ and $C_{\rm NNN}$ to reach larger values at edges as compared to that in bulk, in the nanoribbon geometry considered (see Figs. 7 and 8). A fractional fidelity implies that the wave functions at the edges are more likely to differ from that of an edgeless configuration. This leaves room for the possibility of the lowest quasienergy state to contribute to the conducting edge modes, which indicates gaplessness of the spectrum. We know that the entanglement entropy of a short-ranged gapped system shows areal law behavior for the ground-state entanglement [43], whereas for a gapless system a logarithmic correction is added to that with prefactor proportional to the central charge of the corresponding conformal field theory at the critical point [44]. This makes entanglement at the gapless point to be higher than that of a gapped regime. We find that the entanglement measure of two-qubit concurrence, that we calculate here, also demonstrates similar behavior and produces larger concurrences at the edges than within the bulk.

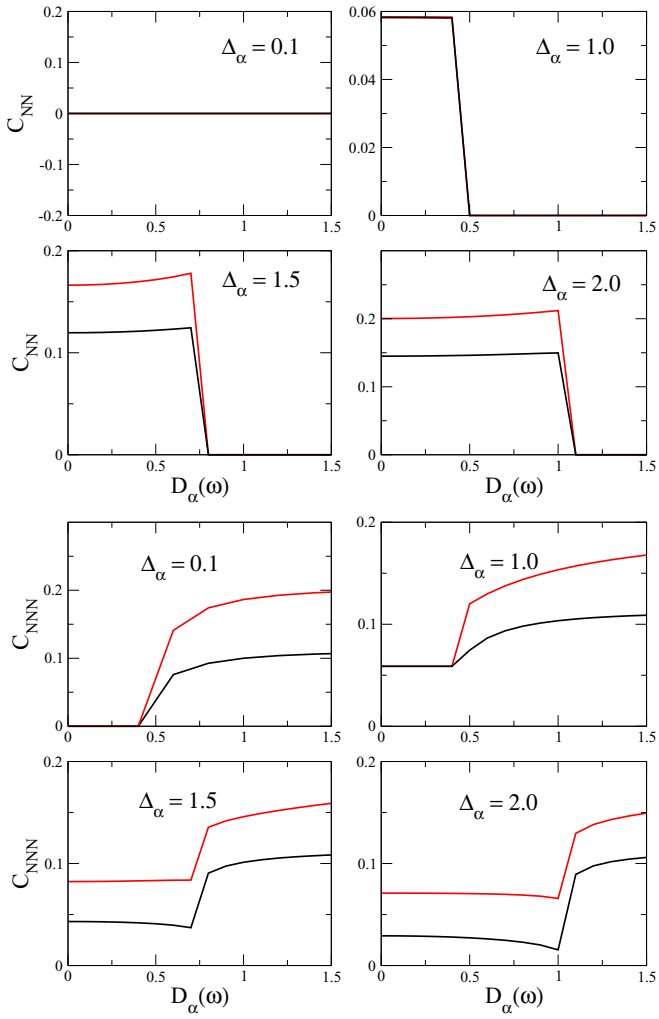

FIG. 8. (Top) C_{NN} and (bottom) C_{NNN} versus $D_\alpha(\omega)$, for fixed Δ_α values, within the bulk (black lines) and at the edges (red lines) on a $L = 18$ size lattice with PBC along x and OBC along y.

V. CONCLUSION

In this work, we have studied spin-spin entanglement in a Floquet system arising out of a FMHS model in a honeycomb lattice irradiated via circularly polarized light. Although this work can be termed as a simple study of entanglement for a spin-$\frac{1}{2}$ XXZ model with NNN DMI on a honeycomb lattice, the easy synthetic tunability of the Floquet system makes this work stand out firmly of the rest for we have the freedom to adjust the parameters of the Hamiltonian. We find that just by varying the amplitude and frequency of irradiation, and not directly modifying the anisotropy or DMI strengths as such, can lead to a plethora of interesting findings, in two-spin ground state as well as thermal concurrences. First, when ω is very large (as compared to J and $\Delta_0 J$), the DMI contribution is negligible and increasing the field strength reduces the spin anisotropy Δ_α. For the easy-planar scenario, reduction of Δ_α comes with decrease (increase) of C_{NN} (C_{NNN}). This occurs as Δ_α quantify interactions between NN spin pairs as well as due to the monogamy of entanglement. Across the Heisenberg point corresponding to the Floquet model, a transition develops from entangled to unentangled NN and NNN spin pairs. If the original spin anisotropy Δ_0 is barely above unity, high-frequency irradiation can make the system unentangled, producing separable product states in the lowest-energy eigenfunctions.

Now, as the frequency becomes intermediate so as to make $D_\alpha(\omega)$ appreciable, the system becomes topological. We see no coincidence between topological and entanglement transitions occurring there. In fact, this is not surprising as our working model obtained from the Floquet theory comprises of short-range interaction/spin fluctuations alone and, hence, unlike in long-range entangled fractional Hall systems [45], we do not see any immediate entangling or disentangling as the DMI term is turned on. However, we notice interesting nontrivial entanglement features in presence of the DM term. The easy-axis Floquet FMHS system produces nonzero C_{NNN} beyond a cutoff D value, as the DM term competes with the NN spin-flip term of the Hamiltonian. For the easy-planar case, both C_{NN} and C_{NNN} are nonzero without a DM term. Here, also C_{NNN} shoots up to a higher value beyond a cutoff $D_\alpha(\omega)$ while C_{NN} reduces down to zero. When we vary the field strength (which is proportional to α), we find that we can choose to have convenient parameters so that sudden death and revival/rebirth of entanglement can be observed. Thus, smooth optical tuning (i.e., altering α and hence the field strength) can result in interesting abrupt changes in the entanglement as easy-axis and easy-planar Floquet system shows different entanglement behavior.

Other than the bulk, we also study a zigzag edged configuration and probe the effect of high-frequency irradiation on that. We find that the lowest quasienergy state differs due to the development of edges in the easy-planar Floquet system and causes the concurrence measures to be higher at the edges as compared to that within the bulk.

Ours is an important piece of work as the concurrence patterns obtained can be useful in extracting quantum information from various QMBS. For example, controlled creation or destruction of entanglement via tuning concurrence of the Floquet states has already been shown for periodically driven coupled flux qubits [46]. Structures of entanglement for both surface and bulk states are examined in the topological insulator Bi_2Te_3 [47] or the full density matrix of two-qubit systems have been measured experimentally and the corresponding concurrence and fidelity computed [48].

We also study thermal concurrence in our Floquet system and demonstrate how the system entanglement steadily decreases with the temperature. Our thermal concurrence results also add important insight to the low-temperature entanglement behavior in QMBS. Down the line, one can also explore the effect of transverse (normal to easy direction) magnetic field on the spins that sometimes witness enhancement of thermal entanglement with temperature [49] (which is not the usual behavior). Besides, it will also be interesting to quantify the quantum coherence [50] or perform the Bell-state measurement [51] on the entangled Floquet states. In short, we believe that this study may trigger various further analytic as well as experimental researches with possible connection to spintronics and topological computations. Our work contains

important results of a condensed matter system (a magnonic FTI) visualized in the context of quantum information, which is pretty new and promising to the condensed matter community. Lastly, we should mention here that experimentally, quantification of concurrence is possible using different protocols for both pure states [52,53] and mixed states [52] and it will be interesting if that can be pursued for our Floquet system and compared with our numerical results.

ACKNOWLEDGMENTS

S.K. thanks S. Ghosh, S. Mandal, S. Yarlagadda, and K. Sengupta for valuable comments, acknowledges CSIR, India, for the financial support, and IACS, India, for providing computational facilities. Both the authors thank S. Owerre and D. Chowdhury for useful discussion on the work. The authors also acknowledge the anonymous referees for their comments and suggestions that resulted in considerable improvement of the paper.

APPENDIX A: FLOQUET HAMILTONIAN

In a honeycomb lattice, there are two sublattices designated by A and B. Each of those sublattices can be defined using three unit vectors $\mathbf{e_1} = (0, a)$, $\mathbf{e_2} = (-\frac{\sqrt{3}}{2}a, -\frac{a}{2})$, $\mathbf{e_3} = (\frac{\sqrt{3}}{2}a, -\frac{a}{2})$. Let us consider a, the length of the NN bonds to be unity. Figure 1(a) shows the same.

A ferromagnetic XXZ spin-$\frac{1}{2}$ model is given by the Hamiltonian

$$H = -\sum_{\langle\alpha,\beta\rangle}\left[JS_\alpha^z S_\beta^z + \frac{J_\perp}{2}(S_\alpha^+ S_\beta^- + \text{H.c.})\right].$$

Under a Holstein-Primakoff transformation, this takes the form $H = \sum_k \psi_k^\dagger H_k \psi_k$ with $\psi_k = (a_k, b_k)^T$ and $H_k = 3JS[\sigma_0 - \Delta(\sigma_+\gamma_k + \text{H.c.})]$. Here, $\Delta = J_\perp/J$, $\sigma_+ = (\sigma_x + i\sigma_y)/2$ and $\gamma_k = \frac{1}{3}\sum_j e^{-ik.e_j}$. a_k, b_k denote the magnon annihilation operators and σ_i's are Pauli matrices to describe the pseudospins. The energy dispersion becomes $\epsilon_k = 3Js(1 \pm \Delta|\gamma_k|)$ that gives degeneracy at the Dirac points $K_\pm = (\pm\frac{4\pi}{3\sqrt{3}}, 0)$. Also notice that the Dirac nodes appear with nonzero energy $3JS$.

Upon irradiation via circularly polarized light with $E = E_0(\tau\cos(\omega t), \sin(\omega t))$ (with $\tau = \pm 1$), an additional phase is added, due to Aharonov-Casher effect, to the amplitude of the spin-fluctuation term involving sites i and j:

$$\phi_{ij} = \frac{\mathbf{1}}{\hbar c^2}\int_{r_i}^{r_j} \boldsymbol{E}\times\boldsymbol{\mu}\cdot\boldsymbol{dl}, \tag{A1}$$

where spin moment $\boldsymbol{\mu} = g\mu_B\hat{z}$ (g and μ_B are gyromagnetic ratio and Bohr magneton, respectively). This brings in the time dependence as

$$H(t) = -J\sum_{\langle i,j\rangle}\left[S_i^z S_j^z + \frac{\Delta}{2}\left(e^{i\phi_{ij}}S_i^+ S_j^- + \text{H.c.}\right)\right]. \tag{A2}$$

For studying dynamics using Floquet theory, first the Fourier components of the Hamiltonian are obtained and they

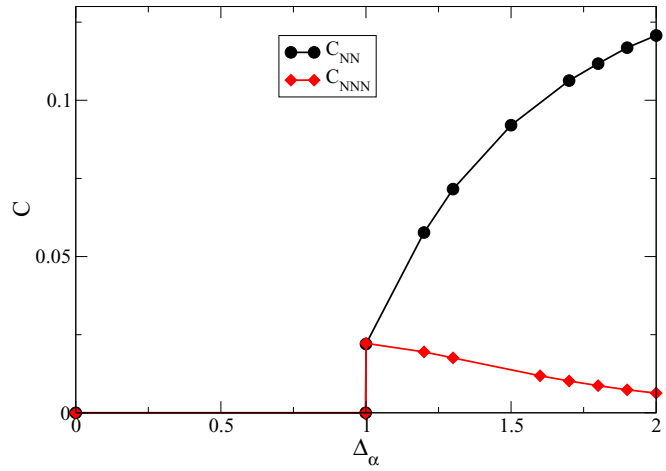

FIG. 9. Finite-size scaling results: Asymptotic values of C_{NN} and C_{NNN} at $\omega \to \infty$ limit.

are given as

$$H^{(n)} = \frac{1}{T}\int_0^T dt\, e^{-in\omega t}H(t)$$
$$= -J\sum_{\langle i,j\rangle}\left[\delta_{n,0}S_i^z S_j^z + \frac{e^{-in\theta_{ij}}}{2}(C_n S_i^+ S_j^- + C_{-n}S_j^+ S_i^-)\right], \tag{A3}$$

where $C_n = J_n(\alpha)\Delta$ and θ_{ij} denotes the angular orientation of the (i, j) bond.

For large ω, we utilize a high-frequency expansion which gives an effective stationary Hamiltonian to the problem: $H_{\text{eff}} = \sum_i H_{\text{eff}}^{(i)}/\omega^i$. For the present case, we obtain $H_{\text{eff}}^{(0)} = H^{(0)} = -J\sum_{\langle i,j\rangle}[S_i^z S_j^z + \frac{C_0}{2}(S_i^+ S_j^- + \text{H.c.})]$ and $H_{\text{eff}}^{(1)} = \sum_{n=1}^{\infty}\frac{1}{n}[H^{(n)}, H^{(-n)}]$. This first-order correction turns out to be $H_{\text{eff}}^{(1)}/\omega = D_F\sum_{ij\ \text{pairs}}\nu_{ij}S_k\cdot(S_i\times S_j)$. Here, $\nu_{ij} = +1\ (-1)$ for $i, j \in A\ (B)$ sublattice and $D_F = \sqrt{3}J^2C_1^2/\omega$. Thus, as long as D_F is not negligible, compared to unity or $C_0/2$ (i.e., the strength of the two terms of $H^{(0)}$), we should consider this first-order correction to the Floquet Hamiltonian. Similar calculations can be seen in Refs. [21,36] as well. Lastly, we want to add here that the second-order correction is proportional to ω^{-2} and if we were to use Eq. (2) for H_F, we must be careful not to choose ω small enough that this term also becomes non-negligible.

APPENDIX B: FINITE-SIZE SCALING

We did a finite-size scaling analysis for concurrences at $\omega \to \infty$ limit involving $L = 12$, 18, and 24 size lattices which shows that the basic feature remains the same other than reducing the absolute values of C_{NN} and C_{NNN} to nonzero smaller values (see Fig. 9). It is not possible to do such analysis in presence of DMI, as $D_\alpha(\omega)$ itself shows some size dependence. But, we can do finite-size scaling analysis for the discontinuous jumps observed in Fig. 3 and our calculations show its values to be 0.012 and 0.020 for $\Delta_\alpha = 1.5$ and 2.0, respectively. This shows that such jump indeed exists in the asymptotic limit.

[1] G. Vidal, Phys. Rev. Lett. **91**, 147902 (2003).
[2] R. Horodechi, P. Horodechi, M. Horodechi, and K. Horodechi, Rev. Mod. Phys. **81**, 865 (2009).
[3] Y. Onose, T. Ideue, H. Katsura, Y. Shiomi, N. Nagaosa, and Y. Tokura, Science **329**, 297 (2010).
[4] L. Zhang, J. Ren, J.-S. Wang, and B. Li, Phys. Rev. B **87**, 144101 (2013).
[5] R. Chisnell, J. S. Helton, D. E. Freedman, D. K. Singh, R. I. Bewley, D. G. Nocera, and Y. S. Lee, Phys. Rev. Lett. **115**, 147201 (2015).
[6] S. A. Owerre, J. Phys.: Condens. Matter **28**, 386001 (2016).
[7] J. Fransson, A. M. Black-Schaffer, and A. V. Balatsky, Phys. Rev. B **94**, 075401 (2016).
[8] S. N. Andrianov and S. A. Moiseev, Phys. Rev. A **90**, 042303 (2014).
[9] A. Khitun, M. Bao, and K. L. Wang, J. Phys. D: Appl. Phys. **43**, 264005 (2010).
[10] J. Simon, H. Tanji, S. Ghosh, and V. Vuletić, Nat. Phys. **3**, 765 (2007).
[11] H. Tanji, S. Ghosh, J. Simon, B. Bloom, and V. Vuletić, Phys. Rev. Lett. **103**, 043601 (2009).
[12] H. P. Specht, C. Nölleke, A. Reiserer, M. Uphoff, E. Figueroa, S. Ritter, and G. Rempe, Nature (London) **473**, 190 (2011).
[13] H. Wang, S. Li, Z. Xu, X. Zhao, L. Zhang, J. Li, Y. Wu, C. Xie, K. Peng, and M. Xiao, Phys. Rev. A **83**, 043815 (2011).
[14] W. K. Wootters, Phys. Rev. Lett. **80**, 2245 (1998).
[15] G. Weick, C. Woollacott, W. L. Barnes, O. Hess, and E. Mariani, Phys. Rev. Lett. **110**, 106801 (2013).
[16] A. B. Khanikaev, S. Hossein Mousaiv, W.-K. Tse, M. Kargarian, A. H. MacDonald, and G. Shvets, Nat. Mater. **12**, 233 (2012).
[17] A. Dutta, U. Divakaran, D. Sen, B. K. Chakraborty, T. N. Rossenbaum, and G. Aeppli, *Quantum Phase Transitions in Transverse Field Spin Models: From Statistical Physics to Quantum Information* (Cambridge University Press, Cambridge & Delhi, 2015).
[18] A. Polkovnikov, K. Sengupta, A. Silva, and M. Vengalattore, Rev. Mod. Phys. **83**, 863 (2011).
[19] S. Kar, B. Mukherjee, and K. Sengupta, Phys. Rev. B **94**, 075130 (2016).
[20] S. Kar, Phys. Rev. B **95**, 085141 (2017).
[21] A. Eckart and E. Anisimovos, New J. Phys. **17**, 093039 (2015).
[22] S. N. Shevchenko, S. Ashhab, and F. Nori, Phys. Rep. **492**, 1 (2010).
[23] J. Cayssol, B. Dora, F. Simon, and R. Moessner, Phys. Status Solidi RRL **7**, 101 (2013).
[24] N. H. Lindner, G. Rafael, and V. Galitski, Nat. Phys. **7**, 490 (2011).
[25] N. H. Lindner, D. L. Bergman, G. Rafael, and V. Galitski, Phys. Rev. B **87**, 235131 (2013).
[26] J.-i. Inoue and A. Tanaka, Phys. Rev. Lett. **105**, 017401 (2010).
[27] Z. Gu, H. A. Fertig, D. P. Arovas, and A. Auerbach, Phys. Rev. Lett. **107**, 216601 (2011).
[28] G. Usaj, P. M. Perez-Piskunow, L. E. F. Foa Torres, and C. A. Balseiro, Phys. Rev. B **90**, 115423 (2014).
[29] O. V. Kibis, K. Dini, I. V. Iorsh, and I. A. Shelykh, Phys. Rev. B **95**, 125401 (2017).
[30] Y. Liu, G. Bian, T. Miller, and T.-C. Chiang, Phys. Rev. Lett. **107**, 166803 (2011).
[31] Z. Yan and Z. Wang, Phys. Rev. Lett. **117**, 087402 (2016).
[32] D. Sinha and S. Kar, Cur. Appl. Phys. **18**, 1087 (2018).
[33] D. Sinha, Europhys. Lett. **115**, 37003 (2016).
[34] A. Menon, D. Chowdhury, and B. Basu, Phys. Rev. B **98**, 205109 (2018); M. Saha and D. Chowdhury, J. Appl. Phys. **122**, 174301 (2017).
[35] P. A. Pantaleon and Y. Xian, J. Phys.: Condens. Matter **29**, 295701 (2017).
[36] S. A. Owerre, J. Phys. Commun. **1**, 021002 (2017).
[37] G.-F. Zhang, Phys. Rev. A **75**, 034304 (2007).
[38] E. R. Gagliano, E. Dagotto, A. Moreo, and F. C. Alcaraz, Phys. Rev. B **34**, 1677 (1986).
[39] Y. Aharonov and A. Casher, Phys. Rev. Lett. **53**, 319 (1984).
[40] S. Kar, K. Wierschem, and P. Sengupta, Phys. Rev. B **96**, 045126 (2017).
[41] Y.-K. Bai, M.-Y. Ye, and Z. D. Wang, Phys. Rev. A **80**, 044301 (2009).
[42] J.-S. Xu, C.-F. Li, M. Gong, X.-B. Zou, C.-H. Shi, G. Chen, and G.-C. Guo, Phys. Rev. Lett. **104**, 100502 (2010); F. Wang, P.-Y. Hou, Y.-Y. Huang, W.-G. Zhang, X.-L. Ouyang, X. Wang, X.-Z. Huang, H.-L. Zhang, L. He, X.-Y. Chang, and L.-M. Duan, Phys. Rev. B **98**, 064306 (2018).
[43] M. Hastings, J. Stat. Mech. (2007) P08024.
[44] P. Calabrese and J. Cardy, J. Stat. Mech. (2004) P060002.
[45] M. Hermanns, Lecture Notes for the 48th IFF Spring School 2017 at the Forschungszentrum Juelich, arXiv:1702.01525 (2017).
[46] A. L. Gramajo, D. Domínguez, and M. J. Sánchez, arXiv:1703.05674.
[47] A. R. Kovela, A. V. Verma, P. K. Panigrahi, and B. Chauhan, arXiv:1704.00579.
[48] M. D. Shulman, O. E. Dial, S. P. Harvey, H. Bluhm, V. Umansky, and A. Yacoby, Science **336**, 202 (2012).
[49] M. C. Arnesen, S. Bose, and V. Vedral, Phys. Rev. Lett. **87**, 017901 (2001); E. Mehran, S. Mahdavifar, and R. Jafari, Phys. Rev. A **89**, 042306 (2014).
[50] C. Radhakrishnan, M. Parthasarathy, S. Jambulingam, and T. Byrnes, Sci. Rep. **7**, 13865 (2017).
[51] S. P. Wallborn, P. H. Souto Ribeiro, L. Davidovich, F. Mintert, and A. Buchleitner, Nature (London) **440**, 1022 (2006).
[52] L. Zhou and Y.- B. Sheng, Entropy **17**, 4293 (2015).
[53] M. Tukiainen, H. Kobayashi, and Y. Shikano, Phys. Rev. A **95**, 052301 (2017).